Evaluation of Satellite-based Upper-troposphere Cloud-top Height Retrievals in Multilayer Cloud Conditions During TC4

Fu-Lung Chang[1], Patrick Minnis[2], J. Kirk Ayers[1], Matthew J. McGill[3], Rabindra Palikonda[1], Douglas A. Spangenberg[1], William L. Smith, Jr.[2], Christopher R. Yost[1]

(1) Science Systems and Applications, Inc., Hampton, Virginia
(2) NASA Langley Research Center, Hampton, Virginia
(3) NASA Goddard Space Flight Center, Greenbelt, Maryland

For submission to J. Geophys. Res. Special Issue on TC4

Corresponding author address:
Dr. Fu-Lung Chang
Mail Stop 420, NASA Langley Research Center, Hampton, Virginia 23681
Email: f.chang@larc.nasa.gov

Abstract

Upper-troposphere cloud-top heights (CTHs), restricted to cloud-top pressures (CTPs) < 500 hPa, inferred using four satellite retrieval methods (two improved and two standard ones) are evaluated by applying to the Twelfth Geostationary Operational Environmental Satellite (GOES-12) imagery data during the July-August 2007 Tropical Composition, Cloud and Climate Coupling Experiment (TC4) based in Costa Rica and by comparing with the ER-2 aircraft-based Cloud Physics Lidar (CPL) data taken during 9 days having extensive upper-troposphere cirrus, anvil and convective clouds. The four methods evaluated here are a single-layer CO_2-absorption technique (SCO2AT), a modified CO_2-absorption technique (MCO2AT) for improvements on both single- and multi-layered clouds, a standard version of the Visible Infrared Solar-infrared Split-window Technique (old VISST), and a new version of VISST (new VISST) recently developed to improve cloud property retrievals. As the CPL detected 89% coverage by upper-tropospheric clouds, the SCO2AT, MCO2AT, old VISST, and new VISST retrieved CTPs < 500 hPa in 76, 76, 69, and 74% of the matched pixels, respectively. Most of the differences are due to very thin cirrus and many sub-visible thin-layer clouds at near tropopause detected only by the CPL. The mean upper-tropospheric CTHs for the 9 days are 14.2 (±2.1) km for the CPL and 10.7 (±2.1), 12.1 (±1.6), 9.7 (±2.9) and 11.4 (±2.8) km for the SCO2AT, MCO2AT, old VISST and new VISST, respectively. Compared to the CPL, MCO2AT CTHs had the smallest biases for semitransparent upper clouds in both single- and multi-layered situations whereas the new VISST CTHs had the smallest biases when upper clouds were opaque and optically thick. The biases for all techniques increased with increasing numbers of cloud layers. The transparency of the upper-layer cloud(s) tends to increase with the numbers of cloud layers.

1. Introduction

Passive satellite instruments have long been used for monitoring large-scale cloud systems in time and space. Yet, the retrieved cloud properties are still subject to large uncertainties. Retrievals of cloud-top height (CTH), a fundamental cloud property, are often biased by 1.5 km or more, even for single-layered cloud systems [e.g., *Smith et al.*, 2008]. On average, those errors can exceed 3 km for thin upper-tropospheric cirrus clouds that are semitransparent in the infrared wavelengths. In the presence of multilayer clouds, errors in the retrieved CTHs are often greater due to the assumption of a single-layered cloud employed in operational satellite retrieval techniques. That is, the retrieval methods interpret the spectral radiances from a given scene as being the result of interactions among the radiances leaving the surface and scattering, absorption, and emission by the atmosphere and a cloud at one particular altitude. When a thin, high cloud overlaps a low cloud, the retrieved CTH is typically found somewhere between the two clouds, its value depending mainly on the high-cloud optical depth and the separation of the two cloud layers. To provide more accurate cloud observations for climate monitoring and the development and validation of cloud process models in weather forecasting, it is necessary to employ a different approach to determine CTH. Active sensors, i.e., cloud lidars and radars, at the surface [e.g., *Clothiaux et al.*, 2000], on aircraft [e.g., *McGill et al.*, 2004], and on satellites [*Winker et al.*, 2007; *Stephens and Kummerow*, 2007] are ideal for accurately determining the vertical layering of clouds, but are quite limited temporally or spatially. Until the challenges of actively sensing clouds on large spatial and relatively high-resolution temporal scales are overcome, it is necessary to develop and test new techniques for unscrambling the passively sensed radiances to retrieve more accurate cloud properties for both single- and multi-layer clouds.

Chang et al. [2009] recently developed a modified CO_2-absorption technique (MCO2AT) that uses two spectral channels, centered near 11 and 13.3 μm, to infer the CTH for the highest cloud whether for single- or multilayered conditions. It differs from the traditional single-layer CO_2-absorption technique (SCO2AT) [e.g., *Chahine*, 1974, *McCleese and Wilson*, 1976, *Smith and Platt*, 1978, *Menzel et al.*, 1983] in that it solves for the cloud-top radiating temperature using estimates for the effective background radiances, instead of using the clear-sky background radiances for the solution. Because the new approach utilizes the 11- and 13.3-μm channels on several newer operational geostationary satellites, such as the Twelfth Geostationary Operational Environmental Satellite Imager (GOES-12) [*Schmit et al.*, 2001], it has the potential for improving the inference of the upper-troposphere transmissive cloud properties in both single-layer and multilayer situations at relatively high temporal and spatial resolutions.

The MCO2AT-inferred upper-troposphere CTH has also been used in combinations with a Visible Infrared Solar-infrared Split-window Technique (hereafter referred as the old VISST) [*Minnis et al.*, 1990, 1993, 1995] to develop a new blended VISST (hereafter referred as the new VISST) for improving the GOES-12 retrievals of upper-tropospheric cloud optical and microphysical properties [*Minnis et al.*, 2009a]. The old VISST retrieves the cloud effective radiating temperature T_{eff} based on the single-layer cloud assumption. The effective cloud height Z_{eff} corresponding to T_{eff} is located somewhere within the cloud, lower than the physical cloud top. For optically thick clouds, the old VISST assumes that the top height is equivalent to the effective height. The old VISST employs a reflectance model based on distributions of smooth-faceted hexagonal columns to infer cloud optical depth, which is used to determine the effective radiating temperature from the observed 11-μm brightness temperature. *Minnis et al.* [2009b] also reported that the ozone correction applied to their visible channel retrievals in the old VISST was too large. This over-correction can result in overestimation of the cloud optical depths and, for semi-transparent clouds, an underestimation of CTH. The new VISST differs from the old version in three respects: a reflectance model based on rough-faceted hexagonal columns replaces the smooth-crystal model, the proper ozone correction is applied, and an empirical adjustment is applied to account for the difference between Z_{eff} and CTH. The differences in the results for the old and new VISST versions have not yet been evaluated.

Data taken during the NASA-sponsored Tropical Composition, Cloud, and Climate Coupling (TC4) Experiment conducted from Costa Rica during July and August 2007 [*Toon et al.*, 2009] are ideal for evaluating passive CTH retrievals from geostationary satellite data. The Cloud Physics Lidar (CPL) on the NASA ER-2 high-altitude aircraft made highly accurate CTH measurements during all of the TC4 flight hours. The flights were conducted during daylight and sampled the clouds at most local times, thus providing data at most solar zenith angles and at different points in the diurnal cycle of convection.

To date, the MCO2AT has only been tested against active sensor retrievals over limited mid-latitude regions [*Chang et al.*, 2009]. Much additional testing of the MCO2AT is needed to ensure that it works well in all conditions, including the high-altitude deep convective conditions in the tropics. The improvements in the VISST have not been quantified for any conditions. Since both the old and new VISSTs were used to analyze the same GOES-12 data during TC4 [*Minnis et al.*, 2009a], it should be possible to determine how accurately the new VISST retrieves ice cloud top heights compared to the old VISST and any CO_2-slicing algorithm using the TC4 data.

The primary objective of this paper is to evaluate the upper-troposphere CTHs (< 500 hPa) inferred by the MCO2AT and the new VISST relative to the SCO2AT and old VISST, respectively. The TC4 CPL CTH data serve as the ground truth for all of the retrievals. This study focuses on the upper-troposphere clouds comprised of convective towers, optically-thick, optically-thin anvils and cirrus, as well as many multilayered clouds.

The paper is organized as follows. Section 2 describes the GOES-12 imager and the ER-2 CPL data used in this study. Section 3 describes the different methodologies of the SCO2AT, MCO2AT and the old and new VISST. Section 4 compares the GOES-12 CTH retrievals by using the four techniques, which are evaluated by comparing with the aircraft CPL CTH data obtained during TC4. Analyses and discussions are also provided for optical-thin, optical-thick, and multilayer cloud scenarios. The final section gives the summary and conclusions.

2. Data

2.1 GOES-12 data

The satellite data used are from the GOES-12 imager that is orbiting at 0°N, 75°W. The GOES-12 imager was used to aid mission planning during TC4 and provide high temporal-resolution cloud products for the entire TC4 experimental area [*Minnis et al.*, 2009; *Toon et al.*, 2009]. The GOES-12 imager 10.7- and 13.3-μm channels are used in the SCO2AT and MCO2AT for retrieving upper-troposphere cloud-top pressure (CTP) as presented in Section 3.1. The 0.65-, 3.9-, 10.7- and 13.3-μm channel data are used by both the old and new VISST [*Minnis et al.*, 2009a] for retrieving the cloud effective temperature and cloud-top temperature (CTT) for clouds located at all altitudes as described in Section

3.2. The CTPs from the SCO2AT and MCO2AT and the CTTs from the two VISST algorithms are converted to CTHs using the profiles of atmospheric pressure, temperature and height data obtained from the National Centers for Environmental Prediction (NCEP) Global Forecast System (GFS) dataset [*Kalnay et al.*, 1990; *Kanamitsu et al.*, 1991].

Half-hourly observations of the GOES-12 imagery data taken at approximately 15 and 45 minutes after the UTC hours were obtained during the TC4 experiment in July and August 2007. The half-hourly GOES-12 imager data and the old and new VISST cloud products were taken from the NASA Langley TC4 imagery and cloud product archives [*Minnis et al.*, 2009a; see http://www-angler.larc.nasa.gov/]. Those data have a nominal 4 km × 3.2 km spatial resolution at nadir. The original scanning resolution is about 4 km × 2.3 km (north-south direction × east-west direction) for the 10.7-μm channel and about 8 km × 2.3 km (north-south × east-west) for the 13.3-μm channel.

2.2 CPL data

The NASA ER-2 flew at an altitude of 20 km, well above the highest cloud tops. The CPL is an active lidar used on high-altitude aircraft to measure attenuated backscatter lidar signals at 532- and 1064-nm wavelengths and is highly sensitive to optically-thin cirrus and sub-visible clouds [*McGill et al.*, 2002]. The CPL retrieves cloud and aerosol backscatter and optical properties at 1 s (~200 m along track) horizontal resolution and 30-m vertical resolution. The CPL retrievals provide top and bottom heights of all layers detected by the lidar up to a maximum of 10 layers with accumulated optical depths < ~4. To determine whether the CPL-detected upper-tropospheric cloud is above the 500-hPa pressure level, the CPL uppermost CTHs are also converted to corresponding CTPs using the NCEP GFS atmospheric data.

3. Techniques

3.1 The CO2ATs

Both CO_2-absorption techniques (CO2ATs), i.e., SCO2AT and MCO2AT, use the radiance pair from the 10.7-μm window and the 13.3-μm CO_2-absorption channel to infer upper-troposphere CTH. The CO2AT is based on the well-mixed nature of CO_2 gas in the upper troposphere. The difference between the 10.7- and 13.3-μm upwelling radiances due to the presence of an upper-troposphere cloud is thus used to infer the cloud-top pressure (CTP). However, CO2AT is only useful for retrieving upper-troposphere clouds because the 13.3-μm data loses its sensitivity to low clouds, owing to an increased CO_2-absorption path length from the top of atmosphere (TOA) to the low cloud top. As such, the CO2AT is conservatively restricted to only the CTH retrieved above 500-hPa level (~5.7 km in altitude) to maximize the signal-to-noise ratio and to avoid the effects of variable CO_2-gas concentrations in the lower troposphere.

The SCO2AT applied to the GOES-12 imager data follows the radiance ratio methods described by *McCleese and Wilson* [1976], *Smith and Platt* [1978] and *Wielicki and Coakley* [1981]. For simplicity, let us use the superscript 11 for the 10.7-μm channel and superscript 13 for the 13.3-μm channel.

By assuming cloud reflectance to be negligible at both the 10.7- and 13.3-μm channels, the satellite-observed radiances R_{obs}^{11} and R_{obs}^{13} for the two channels can thus be written as

$$R_{obs}^{11} = \varepsilon_c^{11} R_{ovc}^{11} + (1 - \varepsilon_c^{11}) R_{clr}^{11} \tag{1}$$

$$R_{obs}^{13} = \varepsilon_c^{13} R_{ovc}^{13} + (1 - \varepsilon_c^{13}) R_{clr}^{13}. \tag{2}$$

where $\varepsilon_c = e_c A_c$ denotes an effective cloud emissivity with e_c being the cloud emissivity and A_c being the cloud cover fraction of the imager pixel, R_{ovc} denotes the overcast radiance as $\varepsilon_c = 1$, and R_{clr} denotes the clear-sky radiance as $\varepsilon_c = 0$.

The clear-sky radiances R_{clr}^{11} and R_{clr}^{13} for specified surface temperature T_g and surface pressure P_g are given by

$$R_{clr}^{11}(T_g|P_g) = B^{11}(T_g)\xi^{11}(P_g) + \int_{P_g}^{0} B^{11}(T(P))\frac{d\xi^{11}(P)}{d\ln P}d\ln P \tag{3}$$

$$R_{clr}^{13}(T_g|P_g) = B^{13}(T_g)\xi^{13}(P_g) + \int_{P_g}^{0} B^{13}(T(P))\frac{d\xi^{13}(P)}{d\ln P}d\ln P, \tag{4}$$

where B^{11} and B^{13} denote the Planck functions and $\xi^{11}(P)$ and $\xi^{13}(P)$ denote the transmittances between the TOA (P = 0) and pressure-level P for the two associated channels. Similarly, the overcast radiances R_{ovc}^{11} and R_{ovc}^{13} for specific cloud-top temperature T_c and cloud-top pressure P_c are give by

$$R_{ovc}^{11}(T_c|P_c) = B^{11}(T_c)\xi^{11}(P_c) + \int_{P_c}^{0} B^{11}(T(P))\frac{d\xi^{11}(P)}{d\ln P}d\ln P \tag{5}$$

$$R_{ovc}^{13}(T_c|P_c) = B^{13}(T_c)\xi^{13}(P_c) + \int_{P_c}^{0} B^{13}(T(P))\frac{d\xi^{13}(P)}{d\ln P}d\ln P. \tag{6}$$

The computations in Eqs. (3)-(6) used the atmospheric profile data obtained from the NCEP GFS dataset [*Kalnay et al.*, 1990; *Kanamitsu et al.*, 1991] and the MODTRAN4 radiative transfer code [*Berk et al.*, 1999].

To solve for $T_c|P_c$ with specified $T_g|P_g$, ratios of (1) and (2) are manipulated to yield

$$\frac{R_{obs}^{13} - R_{clr}^{13}(T_g|P_g)}{R_{obs}^{11} - R_{clr}^{11}(T_g|P_g)} = \frac{\varepsilon_c^{13}(R_{ovc}^{13}(T_c|P_c) - R_{clr}^{13}(T_g|P_g))}{\varepsilon_c^{11}(R_{ovc}^{11}(T_c|P_c) - R_{clr}^{11}(T_g|P_g))}. \tag{7}$$

The solution of $T_c|P_c$ can thus be inferred by searching for the calculations of R_{ovc}^{11} and R_{ovc}^{13} that best satisfy (7) for the satellite-observed pair, R_{obs}^{11} and R_{obs}^{13}. The SCO2AT-inferred CTH is then derived by comparing the inferred $T_c|P_c$ to the atmosphere temperature/pressure and height profile data. Note that previous studies often assumed $\varepsilon_c^{11} \cong \varepsilon_c^{13}$ in Eq. (7). Here the relation between ε_c^{11} and ε_c^{13} is determined based on radiative transfer calculations [*Chang et al.*, 2009].

The MCO2AT is a modified version of the SCO2AT. As the SCO2AT assumes clouds are single-layered with a clear-sky background, the MCO2AT determines the effective background radiances R_{ebg}^{11} and R_{ebg}^{13} and their corresponding effective background temperature T_{ebg} and pressure P_{ebg} for the lower cloud in a multilayer cloud situation or for the clear-sky background for single-layer clouds. As such, Eq. (7) is modified in the MCO2AT by

$$\frac{R_{obs}^{13} - R_{ebg}^{13}(T_{ebg}|P_{ebg})}{R_{obs}^{11} - R_{ebg}^{11}(T_{ebg}|P_{ebg})} = \frac{\varepsilon_c^{13}(R_{ovc}^{13}(T_c|P_c) - R_{ebg}^{13}(T_{ebg}|P_{ebg}))}{\varepsilon_c^{11}(R_{ovc}^{11}(T_c|P_c) - R_{ebg}^{11}(T_{ebg}|P_{ebg}))}, \tag{8}$$

where

$$R_{ebg}^{11}(T_{ebg}|P_{ebg}) = B^{11}(T_{ebg})\xi^{11}(P_{ebg}) + \int_{P_{ebg}}^{0} B^{11}(T(P))\frac{d\xi^{11}(P)}{d\ln P}d\ln P \tag{9}$$

$$R_{ebg}^{13}(T_{ebg}|P_{ebg}) = B^{13}(T_{ebg})\xi^{13}(P_{ebg}) + \int_{P_{ebg}}^{0} B^{13}(T(P))\frac{d\xi^{13}(P)}{d\ln P}d\ln P. \tag{10}$$

To solve for $T_c|P_c$ using Eq. (8), the MCO2AT needs to determine $T_{ebg}|P_{ebg}$ using an iterative algorithm as illustrated in Figure 1. In the iterative algorithm, the solution of a SCO2AT-retrieved $T_c|P_c$ is first obtained using Eq. (7). If the SCO2AT $P_c < 500$ hPa, it proceeds to the MCO2AT iterative algorithm to estimate new $T_{ebg}|P_{ebg}$ and infer new $T_c|P_c$ using Eq. (8). Note that the inferred effective background radiance R^{11}_{ebg} is bound between the clear-sky radiance R^{11}_{clr} and the midway radiance ($R^{11}_{clr} + R^{11}_{obs}$)/2 whereas the inferred $T_c|P_c$ is bound by the tropopause [*Chang et al.*, 2009].

3.2 The VISSTs

The VISST matches theoretically computed radiances with the GOES-12 imager-observed radiances at the 0.65-, 3.9-, 10.7-, and 13.3-μm channels to retrieve cloud parameters such as optical depth (OD), effective particle size, water phase, emissivity, effective cloud temperature, pressure and height, etc. In the old VISST [*Minnis et al.*, 1995, 2009b], for clouds with OD > 6, the CTH is inferred from the value of T_{eff} that is retrieved from the 10.7-μm channel with atmospheric correction. For clouds with OD ≤ 6, cloud transmissivity and emissivity are taken into account to infer the effective cloud temperature. Empirical formulae are then applied to determine the CTHs for thin clouds, where the CTH and cloud temperature are related using the temperature and height profile data.

In the new VISST, as detailed in *Minnis et al.* [2009a], the visible-channel ozone transmittance is reduced by 12% and the rough ice crystal models of *Yang et al.* [2008] are used in place of the smooth models used in the old VISST [*Minnis et al.*, 1998]. The former correction should cause OD to decrease by a few percent, while the latter change can cause either an increase or decrease in OD, depending on the viewing and illumination angles. The third correction is based on an empirical model [*Minnis et al.*, 2008] that accounts fro the differences between Z_{eff} and CTH for optically thick clouds. Thus, most of the corrections should result in slightly smaller retrieved optical depths and higher CTHs.

4. Results

4.1 Comparisons of Uper-troposphere CTHs

The CPL and GOES-12 matched data are analyzed from 9 separate ER-2 flight days during the July-August 2007 TC4 experiment. Data from four other days (July 14, 25, 29 and August 9) are not included here because they were taken during transit flights or flights dedicated to measuring boundary layer clouds and/or aerosols. The CPL uppermost CTHs were averaged every 10 s. The averaging time of 10 s implies a ground track of ~2 km since the ER-2 traveled at a speed of ~200 m/s. Each 10-s averaged CPL CTH was matched with collocated GOES-12 pixel data from the two closest imagery scan times, one scanned before and another scanned after the CPL time. Since the GOES-12 imager scans at 30-min intervals, the collocated GOES-12-retrieved CTHs from the two images scanned before and after were then linearly interpolated in time to match the CPL CTH observation. However, when only one image pixel had retrieved CTH, that pixel CTH was treated as a match to the CPL data if the observing time difference between the image pixel and CPL data was less than 3 minutes. If no CTH was retrieved from either the previous or following images, the CPL data were not used. The different times and resolutions of the GOES-12 and CPL cloud data make the comparisons of CTHs from the two measurements somewhat problematic because a cloud could appear or disappear between the 30-min intervals.

Table 1 shows the number of matched CTH data points obtained by the CPL, CO2ATs, and the VISSTs from the nine flights. It shows the total numbers of matched data (N_{match}) and how many of the matched data had a valid CTP < 500 hPa inferred by the CPL (N_{CPL}), CO2ATs (N_{CO2AT}), and old ($N_{\mathrm{VISST\text{-}old}}$) and new VISST ($N_{\mathrm{VISST\text{-}new}}$). Also, the numbers in parentheses for N_{CO2AT}, $N_{\mathrm{VISST\text{-}old}}$ and $N_{\mathrm{VISST\text{-}new}}$ indicate how many data had a retrieved CTP < 500 hPa, but the CPL had not detected that, which could indicate data mismatches or overestimations by the individual satellite techniques. In general, from comparisons of N_{match} and N_{CPL}, the CPL detected large percentages of CTP < 500 hPa (four days had ~100%). Based on N_{CO2AT}, the CO2ATs retrieved large percentages (75-98%) of those upper-troposphere clouds (CTP < 500 hPa), except for July 19 (~49%) and August 6 (~14%). The two versions of VISST also retrieved consistently large percentages of CTP < 500 hPa, where the new VISST showed good agreement with the CO2ATs and the old VISST showed about 10% less than those from the new VISST. There were less than 0.3% of the data where the CPL data had no CTP < 500 hPa, but the CO2ATs and VISSTs had some CTPs < 500hPa as indicated by the numbers in the parentheses.

Figure 2 illustrates the matched CTHs inferred by the new VISST (blue), old VISST (green), MCO2AT (red) and SCO2AT (purple) overlaid on the ER-2 CPL vertical cloud mask data for 4 flight days. Each figure shows a 3-hour period of matched data obtained during the ER-2 flights on August 8 (Fig. 2a), July 31 (Fig. 2b), July 17 (Fig. 2c) and July 19 (Fig. 2d), which were selected to demonstrate different cloud scenarios.

During August 8 (Fig. 2a), the ER-2 flew over several convective cores and anvils. Comparing the data during this flight (12:40:45-17:40:16) when the CO2ATs had valid CTH retrievals (CTP < 500 hPa), the CPL measured a mean (±standard deviations) CTH of 13.9 (±1.4) km whereas the MCO2AT, SCO2AT, new VISST, and old VISST inferred 12.3 (±1.1) km, 10.7 (±1.8) km, 11.4 (±2.5) km, and 9.7 (±2.4) km, respectively. Generally, good agreement among the CPL, MCO2AT, and new-VISST CTHs was found near the convective cores, but away from the cores their CTH differences increased as the anvil cloud optical depths decreased. The MCO2AT CTHs were sometimes a few kilometers lower and the new-VISST CTHs were sometimes much lower. On average, when compared with the MCO2AT, the new-VISST CTHs were lower by 0.9 km, the old-VISST CTHs were lower by 2.6 km, and the SCO2AT CTHs were lower by 1.6 km.

On July 31 (Fig. 2b), the ER-2 flew over some geometrically-thick anvils formed by a large mesoscale complex in the Pacific just off the coast of Costa Rica. The data from this flight (13:15:56-17:19:40) show that when the CO2ATs had valid CTH retrievals, the CPL measured a mean CTH of 16.3 (±0.3) km whereas the MCO2AT, SCO2AT, new VISST and old VISST inferred mean CTHs of 12.8 (±1.7), 12.2 (±2.0), 13.0 (±2.7) and 11.7 (±2.5) km, respectively. While all four techniques underestimated the optically thin anvil CTHs by more than 3 km, differences between their mean CTHs were generally quite small (within 1.3 km) with the new VISST being the highest and the old VISST being the lowest. It was also found that the new VISST had better agreement with the CPL for optically thicker anvils (cf. Fig. 2b) and convective cores (cf. Fig. 2a). This day also had the highest percentages of CTP < 500 hPa retrieved by all four techniques (CO2ATs ~98 %, new VISST ~95% and old VISST ~94%).

On July 17 (Fig. 2c), the ER-2 flew over a large mesoscale complex off the Pacific coast of Costa Rica. Many optically thin cirrus clouds were missed by the four techniques at the beginning of this flight. The CPL-measured CTHs showed large fluctuations over the mesoscale complex causing problems in matching the collocation of the CPL and GOES-12 imager data. The CPL detected CTP < 500 hPa ~94% of the time, compared to about 71, 66, and 60% for the CO2ATs, the new VISST and the old VISST, respectively. For the period 12:59:25-16:44:09 UTC, when CO2ATs retrieved CTP < 500 hPa, the associated mean

CTHs were 12.8±1.8 km (CPL), 12.0±1.5 km (MCO2AT), 10.3±2.2 km (SCO2AT), 10.3±3.1 km (new VISST), and 8.8±3.0 km (old VISST).

On July 19 (Fig. 2d), the ER-2 flew over the cores of several convective systems in the Pacific and then over the Caribbean to measure Sahara dust and low-lying clouds. There were high-altitude sub-visible thin-cirrus clouds lying above the convective systems during the first couple of flight hours. The sub-visible, thin cirrus clouds were generally not well-retrieved by the four satellite techniques, but the new VISST showed significant improvement in the CTH retrievals over the old VISST. Comparing the data when CO2ATs had valid CTP < 500 hPa, the mean CTHs inferred on this day were 14.5 ±1.3 km (CPL), 12.2 ±1.2 km (MCO2AT), 10.5 ±1.9 km (SCO2AT), 11.7 ±2.4 km (new VISST) and 9.2 ±3.0 km (old VISST). The later periods of this flight were mainly over low-lying stratocumulus clouds [*Toon et al.*, 2009]. Overall, the CPL detected ~59% of CTP < 500 hPa during the flight as compared to only ~29%, ~30% and ~25%, detected by the CO2ATs, new VISST, and old VISST, respectively.

On August 6 (Table 1), the CPL detected an extensive, thin layer of sub-visible high-altitude (~15 km) cirrus clouds that occurred high above a deck of low-altitude (~1 km) boundary-layer clouds [*Toon et al.*, 2009]. The sub-visible cirrus clouds were generally missed by the four satellite techniques, leading to the largest differences in Table 1 between N_{CPL} (1694), N_{CO2AT} (230), $N_{\mathrm{VISST\text{-}old}}$ (191) and $N_{\mathrm{VISST\text{-}new}}$ (242). The sub-visible cirrus clouds on this day are responsible for most of the undetected upper-troposphere clouds in the passive retrieval results.

Overall, there were a total of 15,028 matched data points as shown in Table 1. Out of these, ~89% or 13,387 data (N_{CPL}) had CPL-detected CTHs above 500 hPa. There were

~68% (N_{CO2AT} = 10225) that had MCO2AT/SCO2AT-retrieved CTHs above 500 hPa and, among them, some 0.5% (54) in which the CPL detected no CTHs above 500 hPa. The new VISST retrieved ~66% ($N_{VISST\text{-}new}$ = 9883) having CTP < 500 hPa in contrast to ~61% ($N_{VISST\text{-}old}$ = 9134) from the old VISST retrievals. As a result, the CO2ATs retrieved ~76%, the new VISST retrieved ~74% and the old VISST retrieved ~69% of CTPs < 500 hPa when the CPL detected such upper-troposphere clouds (< 500 hPa). The findings are reasonable considering the large fractions of optically very thin cirrus clouds that occurred during the TC4 experiment [*Toon et al.*, 2009]. The lidar system is much more sensitive to thin clouds than the passive sensors on the GOES-12 imager, which results in more detection of high clouds by the CPL.

Figure 3 shows scatter plots comparing the CTHs retrieved from the four satellite techniques to those from the CPL for all 9 flight days when the CO2ATs retrieved CTPs < 500 hPa. The mean CTHs are 14.2 ±2.1, 10.7 ±2.1, 12.1 ±1.6, 9.7 ±2.9, and 11.4 ±2.8 km km for the CPL, SCO2AT (Figure 3a), MCO2AT (Figure 3b), the old VISST (Figure 3c), and the new VISST (Figure 3d), respectively. The corresponding overall mean biases relative to the CPL are −3.5, −2.1, −4.5 km, and −2.8 km. The MCO2AT reduced the mean biases of the SCO2AT by 1.4 km whereas the new VISST reduced the mean biases of the old VISST by 1.7 km. Note that much better agreement between the new VISST and CPL are found for CTH > 14 km. Unlike the new VISST, all of the SCO2AT (Fig. 3a), MCO2AT (Fig. 3b) and old VISST (Fig. 3c) have generally underestimated the CTHs between 14.0-16.5 km.

4.2 Cloud Emissivities and Multilayer Clouds

Figure 4 shows the CTH differences (dz_c) between the CPL and the four passive methods plotted as a function of the MCO2AT-inferred cloud 10.7-μm effective emissivity (ε_c^{11}). Results in the figure were obtained from the 9-day data shown in Figure 3. For more opaque and likely optically thick clouds with ε_c^{11} > 0.95, the mean dz_c were found to be −1.9, −1.4, −2.4, and −0.2 km for the SCO2AT (Figure 4a), MCO2AT (Figure 4b), old VISST (Figure 4c), and new VISST (Figure 4d), respectively. The underestimation of CTH by 1.4-2.4 km for those nearly opaque clouds (except for the new VISST case) are consistent with earlier results found by *Sherwood et al.*, [2004], who showed that the satellite infrared-derived CTHs were 1-2 km below the physical cloud tops detected by lidar instruments. This underestimation appeared to have been largely corrected with the method of *Minnis et al.*, [2008] used in the new-VISST algorithm.

For less opaque clouds with ε_c^{11} < 0.95, the absolute differences increase progressively with decreasing ε_c^{11}. For instance, for semitransparent clouds at ε_c^{11} ~ 0.3, the mean dz_c were found to be −5.1 km (SCO2AT − CPL), −2.8 km (MCO2AT −CPL), −5.7 km (old VISST − CPL) and −3.9 km (new VISST − CPL). Note that the MCO2AT appeared to have more overestimated CTHs for less opaque clouds (ε_c^{11} < 0.8) and have the overall smallest mean dz_c compared to the SCO2AT (Fig. 4a) and two VISSTs (Figs. 4c and 4d).

To examine the impact of multilayer clouds on the retrievals, Figure 5 shows the CTH differences from Fig. 4 plotted as a function of the averaged number of cloud layers (N_{layer}) detected by the CPL. For single-layered clouds (N_{layer} = 1), the associated mean dz_c are −2.5 (SCO2AT), −1.4 (MCO2AT), −3.2 (old VISST) and −1.6 km (new VISST). The absolute mean dz_c of all four techniques increase with increasing N_{layer}, but the MCO2AT shows the smallest mean biases for all single- and multi-layered clouds and it systematically reduces the SCO2AT mean biases by ~40%. However, there appears to be the possibility that the CPL detects more cloud layers because the optical depths of the upper layer(s) are thinner in those cases and, as a result, the greater number of cloud layers may simply be related to more transmissive (smaller ε_c^{11}) upper cloud layer(s). Therefore, the differences need to be examined separately for the different multilayered conditions.

Figures 6-8 present the dz_c as a function of ε_c^{11} by separating the single-layered (Figure 6), two-layered (Figure 7), and multi-layered (Figure 8) clouds. For the single-layered cases, the mean dz_c are fairly constant within each technique until ε_c^{11} falls below 0.5. For $0.5 < \varepsilon_c^{11} < 0.95$, the MCO2AT has the smallest mean dz_c (−0.5 to −1.0 km) and it reduces the SCO2AT absolute mean biases by ~1 km. The new VISST also reduces the absolute mean biases of the old VISST significantly towards larger ε_c^{11}.

For the two-and more-layered cases, their mean differences behaved like those discussed in Fig. 4, except that the two- and more-layered clouds (Figures 7 and 8) showed larger magnitudes of differences than those of the single-layered clouds (Figure 6). The MCO2AT generally has the smallest mean biases among all multilayered clouds with $\varepsilon_c^{11} < 0.9$ and, similarly, it reduces the SCO2AT absolute mean biases by ~40%. Nonetheless, the discrepancies among the SCO2AT, MCO2AT, old VISST and new VISST all increased considerably as ε_c^{11} decreased to values smaller than 0.5 and the discrepancies among the four techniques are greater for the more semitransparent upper-troposphere clouds.

Also, there were 3162 data when the CPL detected CTHs above 500 hPa, but the CO2ATs had no retrieval due to probably thin clouds and/or edges of broken clouds. Among these data, ~50% had VISST-retrieved CTHs and these are plotted in Figure 9a (old VISST) and Figure 9b (new VISST) as compared with the CPL CTHs. Since such cases were very optically thin clouds, it is not surprising to see that most of the VISST CTHs are much too low, especially since there were no MCO2AT/SCO2AT retrievals available. The mean CTHs are 13.2 (±2.6) km for the CPL, 3.3 (±2.4) km for the old VISST, and 3.9 (±2.7) for the new VISST. Although the mean improvement is small, more data in the new VISST showed fairly good CTHs retrievals. Nevertheless, it is clear that these apparently optically thin cloud retrievals should be used very cautiously. Although the VISST sometimes detects clouds with optical depths less than 0.1, the retrieved values are highly inaccurate.

To summarize, among the four techniques, the MCO2AT generally produces better agreement with the CPL for optically thin clouds when CTPs < 500 hPa were retrieved. The MCO2AT also has the best performance for all upper-transmissive clouds that are in single- and multilayered conditions. It enhances the mean SCO2AT CTH by ~1 km and, thus, reduces the mean SCO2AT biases by ~40%. The new VISST produces more accurate CTHs for the tropical upper-tropospheric clouds compared to the old VISST. The new correction for Z_{eff} to CTH employed in the new VISST algorithm yielded a nearly unbiased result for optically thick clouds. The new ozone and ice crystal models also employed in the new VISST increased the overall detection of optically thin clouds as well as enhanced the CTH retrievals for those optically thin clouds.

5. Summary and Conclusions

Nine days of daytime upper-troposphere cloud-top height (CTH) measurements obtained from GOES-12 imager data and the ER-2 CPL data during the July-August 2007

TC4 were compared to evaluate four satellite retrieval techniques for processing enhanced satellite single-layer and multilayer cloud property retrieval products at NASA Langley Research Center (LaRC) [*Minnis et al.*, 2009a]. The comparisons focused on upper-tropospheric clouds retrieved with CTP < 500 hPa using a standard single-layered CO_2-absorption technique (SCO2AT), a modified CO_2-absorption technique (MCO2AT), an earlier version of a Visible-Infrared-Shortwave-Split-window Technique (old VISST), and a recently-improved version of the VISST (new VISST).

The evaluations of the four satellite techniques are important because the old VISST and MCO2AT algorithms are currently operating together to provide satellite cloud property retrieval products at LaRC for single and multilayered clouds and the new VISST algorithm is expected to improve those cloud products. In comparisons with the CPL CTHs, the mean CTH biases with the MCO2AT are smaller by a factor of ~1.7 than those with the SCO2AT whereas the mean biases with the new VISST are smaller by a factor of ~1.6 than those with the old VISST. Overall, the CPL detected ~89% CTPs < 500 hPa whereas the SCO2AT, MCO2AT, old VISST, and new VISST retrieved 76, 76, 69, and 74% of those, respectively. When both the CPL and CO2ATs detected CTPs < 500 hPa, the mean CTHs from the CPL, SCO2AT and MCO2AT are 14.2 (±2.1), 10.7 (±2.1) and 12.1 (±1.6) km whereas the associated mean CTHs from the old and new VISSTs are 9.7 (±2.9) and 11.4 (±2.8) km, respectively. These results are encouraging when one considers the large percentages of upper-tropospheric semitransparent clouds found during TC4. Although the MCO2AT CTHs are generally in better agreement with the CPL data, their CTHs are on average ~2.1 km lower than the CPL CTHs. The mean bias of 2.1 km found here for the TC4 tropical clouds is twice as large as the mean bias of ~1 km shown in *Chang et al.* [2009] who evaluated the MCO2AT-inferred CTHs for midlatitude clouds between 20°N-55°N. The larger mean bias found here is likely owing to the high occurrences of optically thin cirrus clouds during TC4. However, both studies show that the MCO2AT mean CTH is ~1.4 km higher than the SCO2AT.

Overall, the new VISST algorithm produces more accurate CTHs for optically thick clouds compared to the old VISST algorithm. The new correction of CTHs in the new VISST algorithm yielded a nearly unbiased result for optically thick clouds. The CTHs from the new VISST for thinner clouds also increased for all cloud emissivities as compared with their old VISST counterparts. An additional benefit of the new VISST algorithm is its enhanced detection of optically thin cirrus clouds by more than 5% compared to the old VISST algorithm.

As demonstrated in this study, the main cause of the CTH biases in all four satellite techniques applied to the GOES-12 imager data is associated with the semitransparencies of tropical upper-tropospheric clouds. Their retrieval biases increased progressively as the cloud effective emissivity decreased below about 0.5. Further analysis also showed that the mean biases increased from single-layered cloud cases to multilayered cloud cases in all four techniques, but larger uncertainties were still associated mainly with the semitransparent clouds having emissivities less than ~0.5. It was found that the mean biases increased with the number of cloud layers detected by the CPL, which implies that as the numbers of the cloud layers increased, so too did the semitransparency of the upper layer(s) in those multilayered cloud cases.

From the perspective that the MCO2AT uses only the infrared data at 10.7- and 13.3-μm channels, the technique can be applied equally for daytime and nighttime observations and is applicable to the Spinning Enhanced Visible and Infrared Imager (SEVIRI) on *Meteosat*-8 and -9, the Moderate-resolution Imaging Spectroradiometer (MODIS) on *Terra* and *Aqua*, and the upcoming GOES-R imager series [*Schmit et al.*, 2005]. Another application of the MCO2AT is for multilayer cloud retrieval as shown in *Chang and Li* [2005]. The MCO2AT in conjunction with the new VISST has recently been developed for an integrated multilayer cloud retrieval algorithm as illustrated in the results of *Minnis et al.* [2009a]. Future work requires more validation studies for more assessment of the MCO2AT, the new VISST, and the multilayer retrieval technique.

Acknowledgements

This research was supported by the NASA Radiation Science Program TC4 project, the NASA Applied Sciences Program, the Department of Energy Atmospheric Radiation Measurement Program through Interagency Agreement, DE-AI02-07ER64546, and the NOAA Center for Satellite Applications and Research GOES-R program.

References

Berk, A., et al. (1999), MODTRAN4 v. 2.0 User's Manual, Air Force Geophysics Laboratory Tech. Rep. AFGL-TR-89-0122, 98 pp., Air Force Mat. Comm., Hanscomb AFB, Mass.

Chahine, M. T. (1974), Remote sounding of cloudy atmospheres. I. The single cloud layer, *J. Atmos. Sci.*, *31*, 233-243.

Chang, F.-L., and Z. Li (2005), A new method for detection of cirrus overlapping water clouds and determination of their optical properties, *J. Atmos. Sci.*, *62*, 3993–4009.

Chang, F.-L., P. Minnis, B. Lin, M. M. Khaiyer, R. Palikonda, and D. A. Spangenberg (2009), A modified method for inferring upper-troposphere cloud-top height using the GOES-12 imager 10.7- and 13.3-μm data, *J. Geophys. Res.*, in revision.

Clothiaux, E. E., T. P. Ackerman, G. G. Mace, K. P. Moran, R. T. Marchand, M. Miller, and B. E. Martner (2000), Objective determination of cloud heights and radar reflectivities using a combination of active remote sensors at the ARM CART Sites, *J. Appl. Meteorol.*, *39*, 645-665.

Kalnay, E., M. Kanamitsu, and W. E. Baker (1990), Global numerical weather prediction at the National Meteorological Center, *Bull. Am. Meteorol. Soc.*, *71*, 1410-1428.

Kanamitsu, M., and coauthors (1991), Recent changes implemented into the Global Forecast System at NMC, *Weather and Forecasting*, *6*, 425-435.

McCleese, D. J., and L. S. Wilson (1976), Cloud top heights from temperature sounding instruments, *Q. J. R. Meteorol. Soc.*, *102*, 781-790.

McGill, M. J., D. L. Hlavka, W. D. Hart, J. D. Spinhirne, V. S. Scott, and B. Schmid (2002), The Cloud Physics Lidar: Instrument description and initial measurement results, *Applied Optics*, *41*, 3,725-3,734.

McGill, M. J., L. Li, W. D. Hart, G. M. Heymsfield, D. L. Hlavka, P. E. Racette, L. Tian, M. A. Vaughan, and D. M. Winker (2004), Combined lidar-radar remote sensing: Initial results from CRYSTAL-FACE, *J. Geophys. Res.,* 109, doi: 10.1029/2003JD004030.

Menzel, W. P., W. L. Smith, and T. R. Stewart (1983), Improved cloud motion vector and altitude assignment using VAS, *J. Climate Appl. Meteorol.*, *22*, 377-384.

Minnis, P., D. P. Kratz, J. A. Coakley, Jr., M. D. King, D. Garber, P. Heck, S. Mayor, D. F. Young, and R. Arduini (1995), Cloud optical property retrieval (Subsystem 4.3), Clouds and the Earth's Radiant Energy System (CERES), Algorithm Theoretical Basis Document, 3, Cloud analyses and radiance inversions (Subsystem 4), NASA RP 1376, 3, edited by CERES Science Team, pp. 135-176.

Minnis, P., D. P. Garber, D. F. Young, R. F. Arduini, and Y. Takano (1998), Parameterization of reflectance and effective emittance for satellite remote sensing of cloud properties, *J. Atmos. Sci.*, *55*, 3313-3339.

Minnis, P., C. R. Yost, S. Sun-Mack, and Y. Chen (2008), Estimating the physical top altitude of optically thick ice clouds from thermal infrared satellite observations using CALIPSO data, *Geophys. Res. Lett.*, *35*, L12801, doi:10.1029/2008GL033947.

Minnis, P., and coauthors (2009a), Cloud properties determined from GOES and MODIS data during TC4, submitted to *J. Geophys. Res.*, this issue.

Minnis, P., S. Sun-Mack, and Co-authors (2009b), Cloud property retrievals for CERES using TRMM VIRS and Terra and Aqua MODIS data. *IEEE Trans. Geosci. Remote Sens.*, submitted.

Rossow, W. B., and R. A. Schiffer (1999), Advances in understanding clouds from ISCCP, *Bull. Am. Meteorol. Soc.*, *80*, 2261-2287.

Schmit, T. J., E. M. Prins, A. J. Schreiner, and J. J. Gurka (2001), Introducing the GOES-M imager, *National Weather Assoc. Digest*, *25*, 28-37.

Schmit, T. J., M. M. Gunshor, W. P. Menzel, J. J. Gurka, J. Li, and A. S. Bachmeier (2005), Introducing the next-generation Advanced Baseline Imager on GOES-R, *Bull. Am. Meteorol. Soc.*, *86*, 1079-1096.

Sherwood, S. C., J.-H. Chae, P. Minnis, and M. McGill (2004), Underestimation of deep convective cloud tops by thermal imagery, *Geophys. Res. Lett.*, *31*, 10.1029/2004GL019699.

Smith, W. L., and C. M. R. Platt (1978), Comparison of satellite-deduced cloud heights with indications from radiosonde and ground-based laser measurements, *J. Appl. Meteorol.*, *17*, 1796-1802.

Smith, W. L., Jr., P. Minnis, H. Finney, R. Palikonda, and M. M. Khaiyer (2008), An evaluation of operational GOES-derived single-layer cloud top heights with ARSCL over the ARM Southern Great Plains site, *Geophys. Res. Lett.*, *35*, L13820, doi:10.1029/2008GL034275.

Stephens, G. L., and C. D. Kummerow (2007), The Remote Sensing of Clouds and Precipitation from Space: A Review, *J. of Atmos. Sci.*, 64, 3742–3765.

Toon, O. B., and Co-authors (2009), Planning and implementation of the Tropical Composition, Cloud and Climate Coupling Experiment (TC4), *J. Geophys. Res.*, this issue.

Wielicki, B. A., and J. A. Coakley Jr. (1981), Cloud retrieval using infrared sounder data: Error analysis, *J. Appl. Meteorol.*, *20*, 157-169.

Winker, D. M., W. H. Hunt, and M. J. McGill (2007), Initial performance assessment of CALIOP, Geophys. Res. Lett., 34, L19803, doi:10.1029/2007GL030135.

Yang, P., G. W. Kattawar, G. Hong, P. Minnis, and Y. X. Hu (2008), Uncertainties associated with the surface texture of ice particles in satellite-based retrieval of cirrus clouds: Part I. Single-scattering properties of ice crystals with surface roughness, *IEEE Trans. Geosci. Remote Sens.*, 46(7), 1940-1947.

Table 1 ER-2 flight dates, time periods, numbers of CPL and GOES12-imager matched data points (N_{match}) and numbers of the data points having valid CTP < 500 hPa from the CPL (N_{CPL}), the CO2ATs (N_{CO2AT}) and the two VISSTs ($N_{VISST\text{-}old}$, $N_{VISST\text{-}new}$). In parentheses indicate the numbers of data points having valid CTP < 500 hPa, but the CPL does not detect a CTP < 500 hPa.

Date	Time	N_{match}	N_{CPL}	N_{CO2AT}	$N_{VISST\text{-}old}$	$N_{VISST\text{-}new}$
Jul. 17	12:59:25-16:44:09	1348	1262	963 (7)	806 (5)	890 (7)
Jul. 19	12:55:21-17:51:41	1777	1053	513 (0)	450 (1)	528 (1)
Jul. 22	12:29:23-17:15:45	1717	1628	1475 (31)	1259 (10)	1417 (19)
Jul. 24	12:11:31-18:14:42	2179	1745	1292 (16)	1225 (13)	1312 (14)
Jul. 31	13:15:56-17:19:40	1462	1462	1435 (0)	1379 (0)	1396 (0)
Aug. 3	13:49:16-17:51:17	1452	1452	1349 (0)	1113 (0)	1213 (0)
Aug. 5	13:21:29-16:58:11	1298	1298	1244 (0)	1143 (0)	1218 (0)
Aug. 6	12:40:47-18:14:03	1999	1694	230 (0)	191 (3)	242 (1)
Aug. 8	12:40:45-17:40:16	1796	1793	1724 (0)	1568 (0)	1667 (0)

Figure Captions

Fig. 1 Schematic diagram for illustrating the SCO2AT and MCO2AT algorithms.

Fig. 2 Comparisons of the different CTHs inferred from the GOES-12 imager data using the new-VISST (blue), old-VISST (green), SCO2AT (purple) and MCO2AT (red). The CPL cloud vertical mask is shown in grey. (a) for August 8 between 12:40:45-15:40:45 UTC. (b) for July 31 between 13:15:56-16:15:56 UTC. c) for July 17 between 12:59:25-15:59:25 UTC. d) for July 19 between 12:55:21-15:55:21 UTC.

Fig. 3 Comparisons of CTHs inferred from the GOES-12 imager and the CPL data. (a) for SCO2AT vs CPL. (b) for MCO2AT vs CPL. (c) for old-VISST vs CPL. (d) for new-VISST vs CPL.

Fig. 4 The CTH difference dz_c as a function of the 10.7-μm cloud effective emissivity ε_c^{11}. (a) for the SCO2AT minus CPL. (b) for the MCO2AT minus CPL. (c) for the old-VISST minus CPL. (d) for the new-VISST minus CPL. Thick-grey lines represent the running means.

Fig. 5 The CTH difference dz_c as a function of the number of cloud layers N_{layer}. (a) for the SCO2AT minus CPL. (b) for the MCO2AT minus CPL. (c) for the old-VISST minus CPL. (d) for the new-VISST minus CPL. Thick-grey lines represent the running means.

Fig. 6 Same as in Fig. 4, except for the single-layered clouds.

Fig. 7 Same as in Fig. 4, except for the two-layered clouds.

Fig. 8 Same as in Fig. 4, except for the multilayered ($N_{layer} > 2$) clouds.

Fig. 9 Comparisons of the old-VISST (a) and new-VISST (b) CTHs with the CPL CTH for the data when there are no SCO2AT/MCO2AT retrievals.

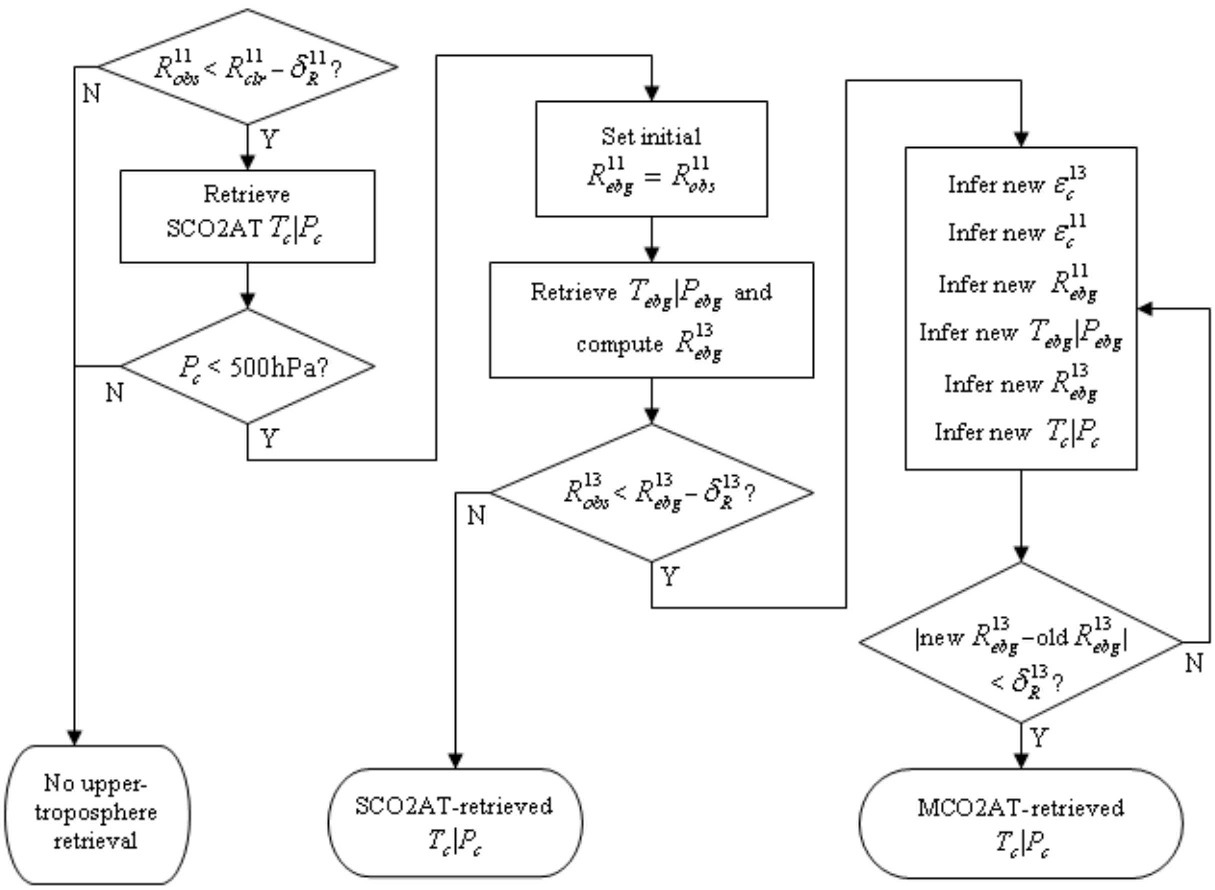

Fig. 1 Schematic diagram for illustrating the SCO2AT and MCO2AT algorithms.

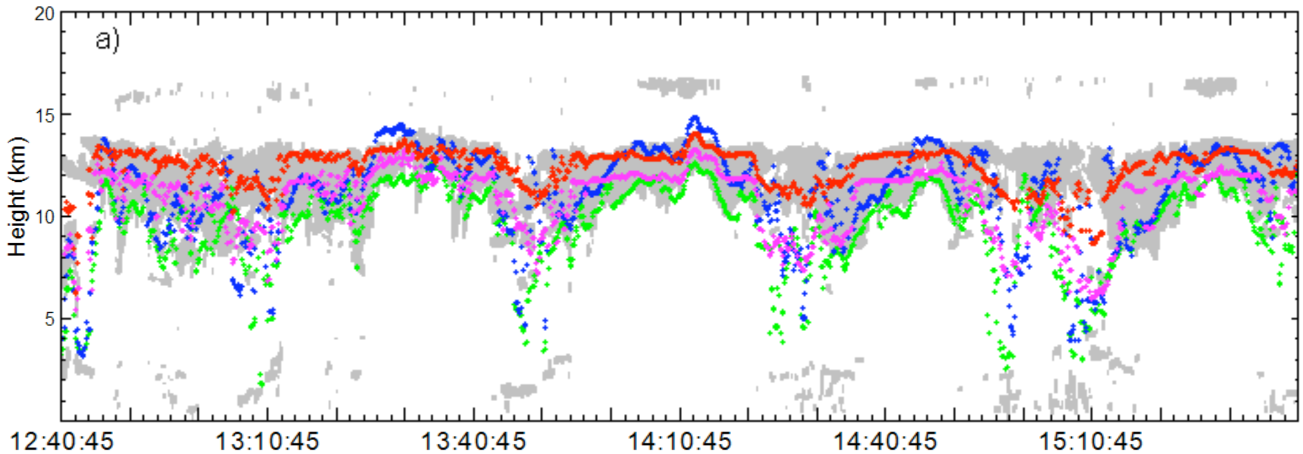

Fig. 2 Comparisons of the different CTHs inferred from the GOES-12 imager data using the new-VISST (blue), old-VISST (green), SCO2AT (purple) and MCO2AT (red). The CPL cloud vertical mask is shown in grey. (a) for August 8 between 12:40:45-15:40:45 UTC. (b) for July 31 between 13:15:56-16:15:56 UTC. c) for July 17 between 12:59:25-15:59:25 UTC. d) for July 19 between 12:55:21-15:55:21 UTC.

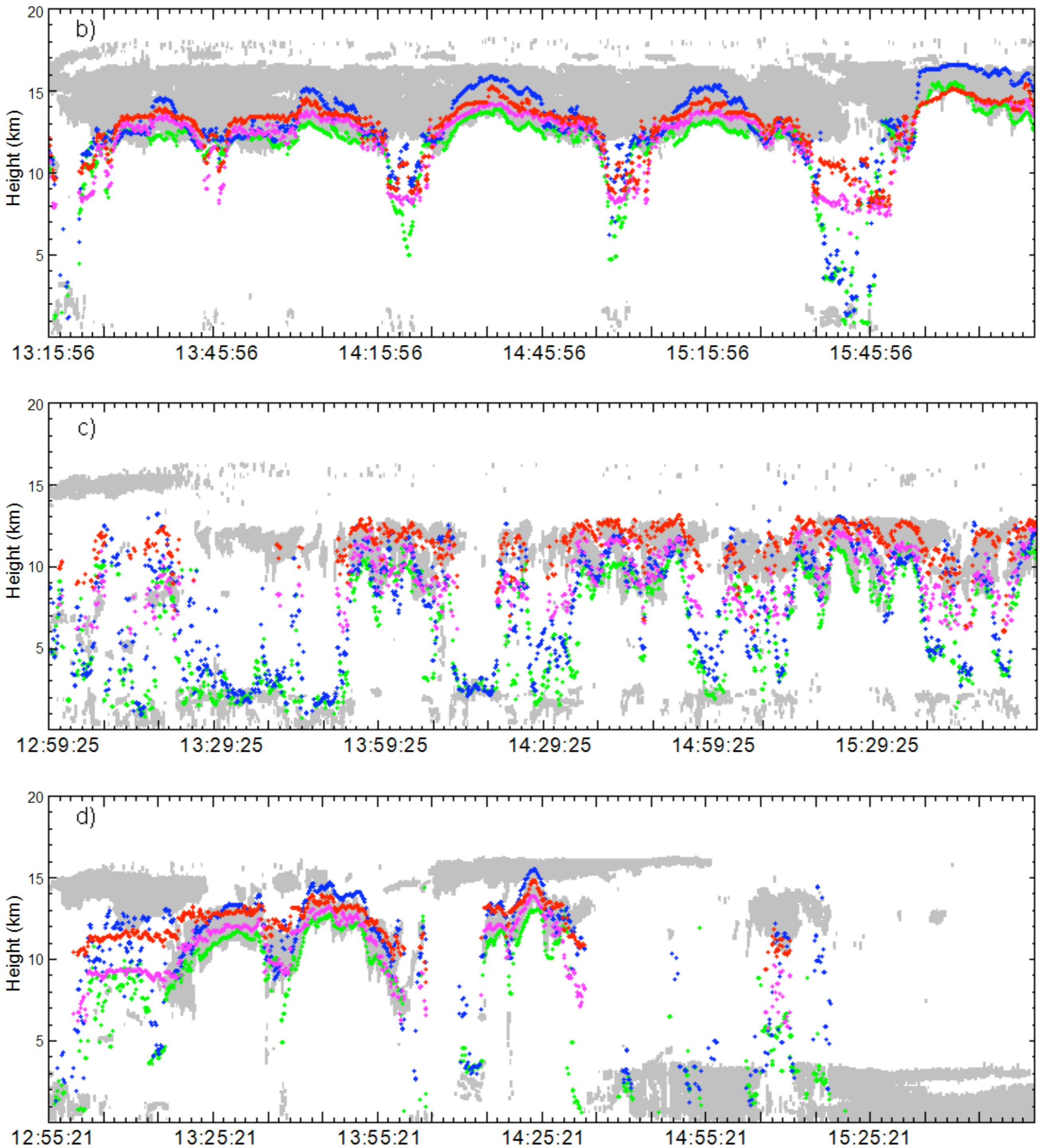

Fig. 2 (continued)

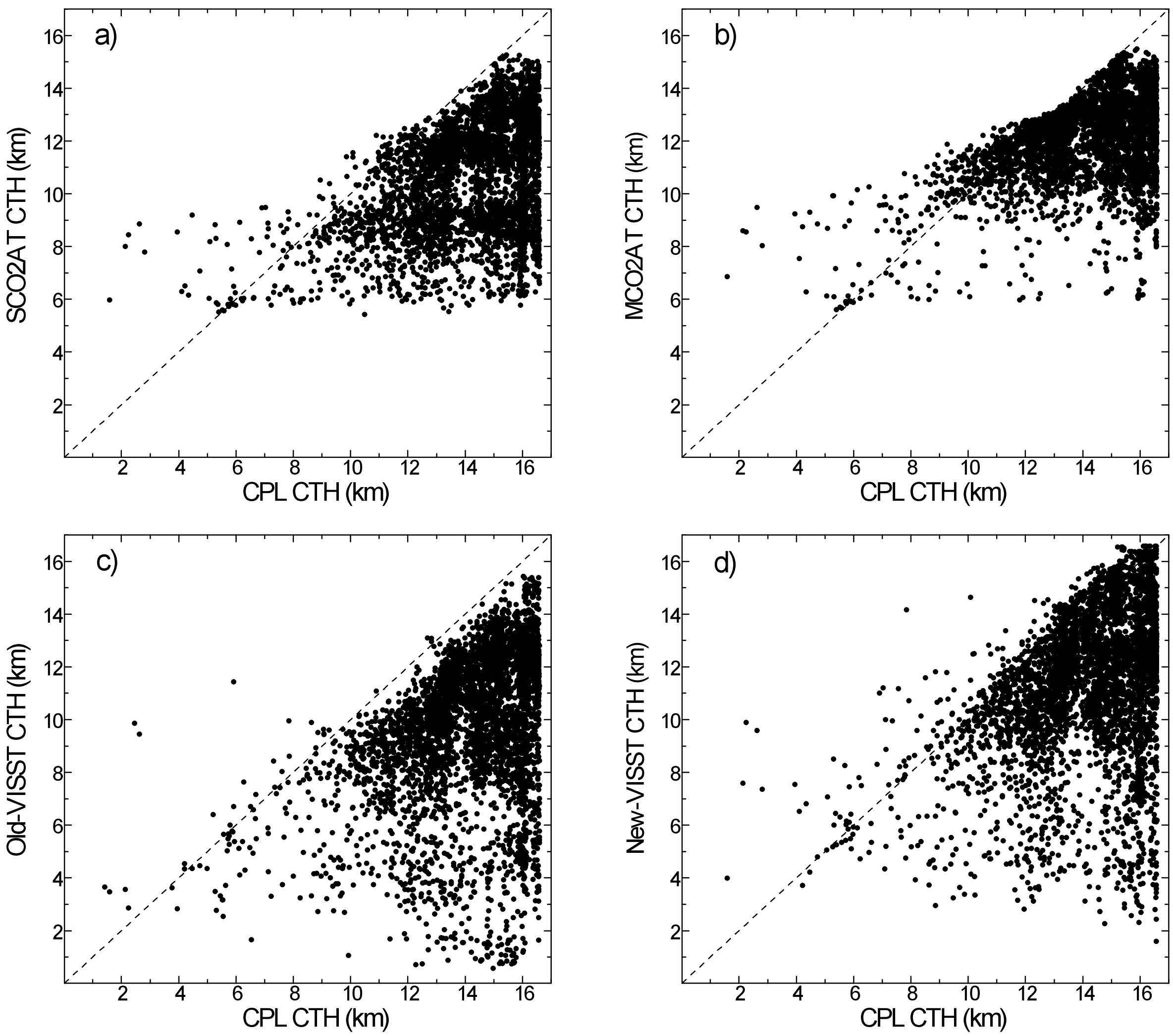

Fig. 3 Comparisons of CTHs inferred from the GOES-12 imager and the CPL data. (a) for SCO2AT vs CPL. (b) for MCO2AT vs CPL. (c) for old-VISST vs CPL. (d) for new-VISST vs CPL.

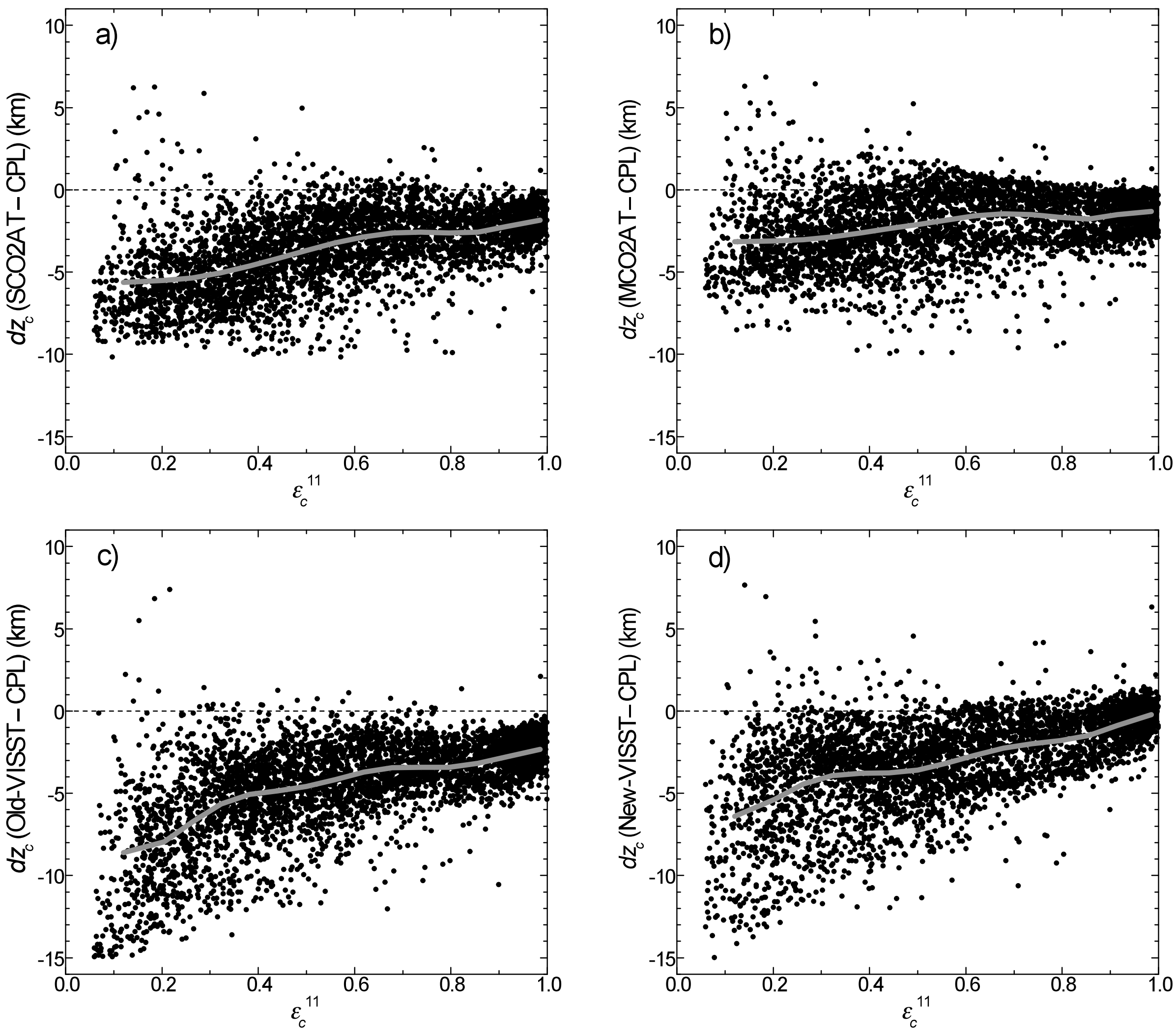

Fig. 4 The CTH difference dz_c as a function of the 10.7-μm cloud effective emissivity ε_c^{11}. (a) for the SCO2AT minus CPL. (b) for the MCO2AT minus CPL. (c) for the old-VISST minus CPL. (d) for the new-VISST minus CPL. Thick-grey lines represent the running means.

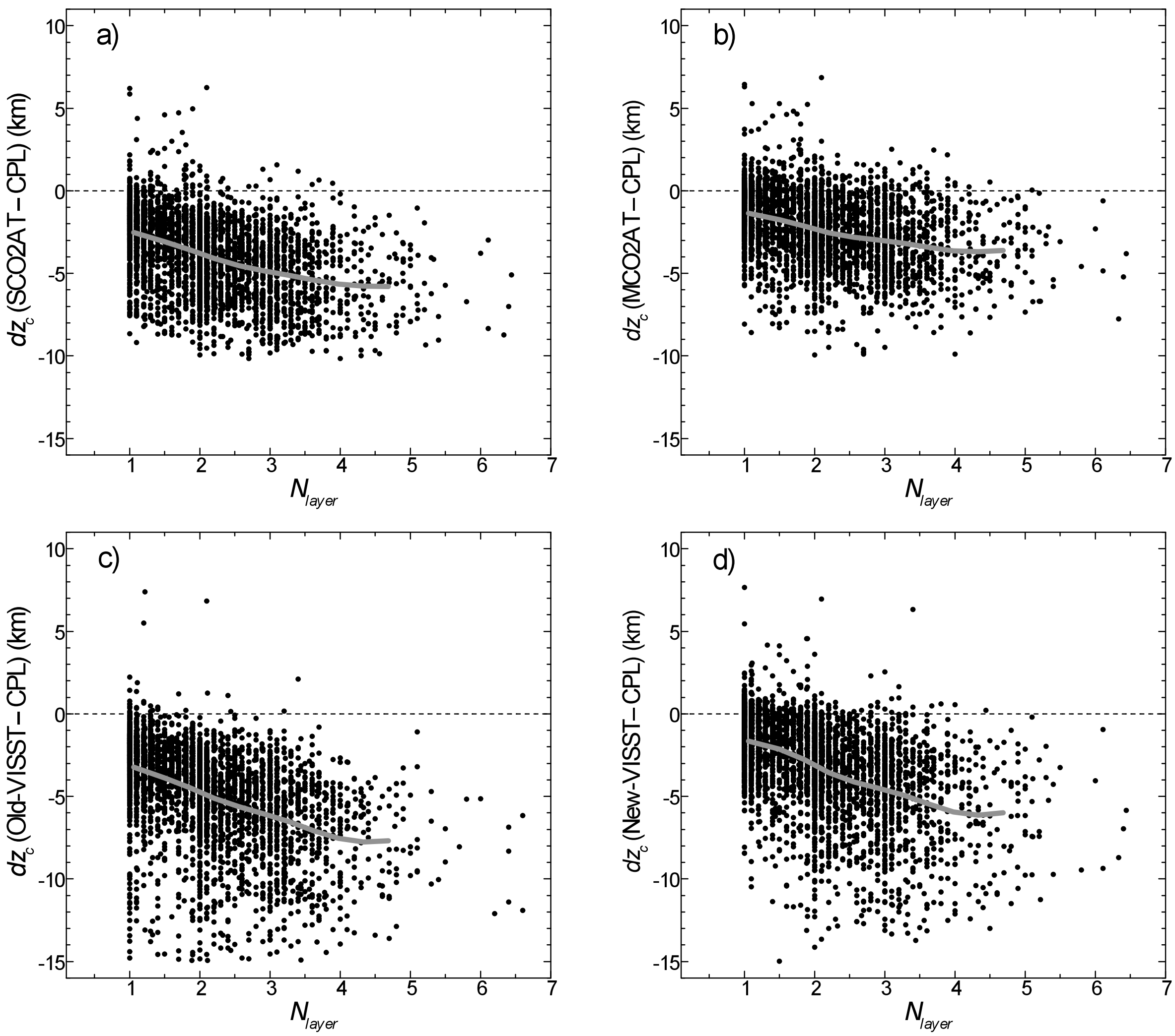

Fig. 5 The CTH difference dz_c as a function of the number of cloud layers N_{layer}. (a) for the SCO2AT minus CPL. (b) for the MCO2AT minus CPL. (c) for the old-VISST minus CPL. (d) for the new-VISST minus CPL. Thick-grey lines represent the running means.

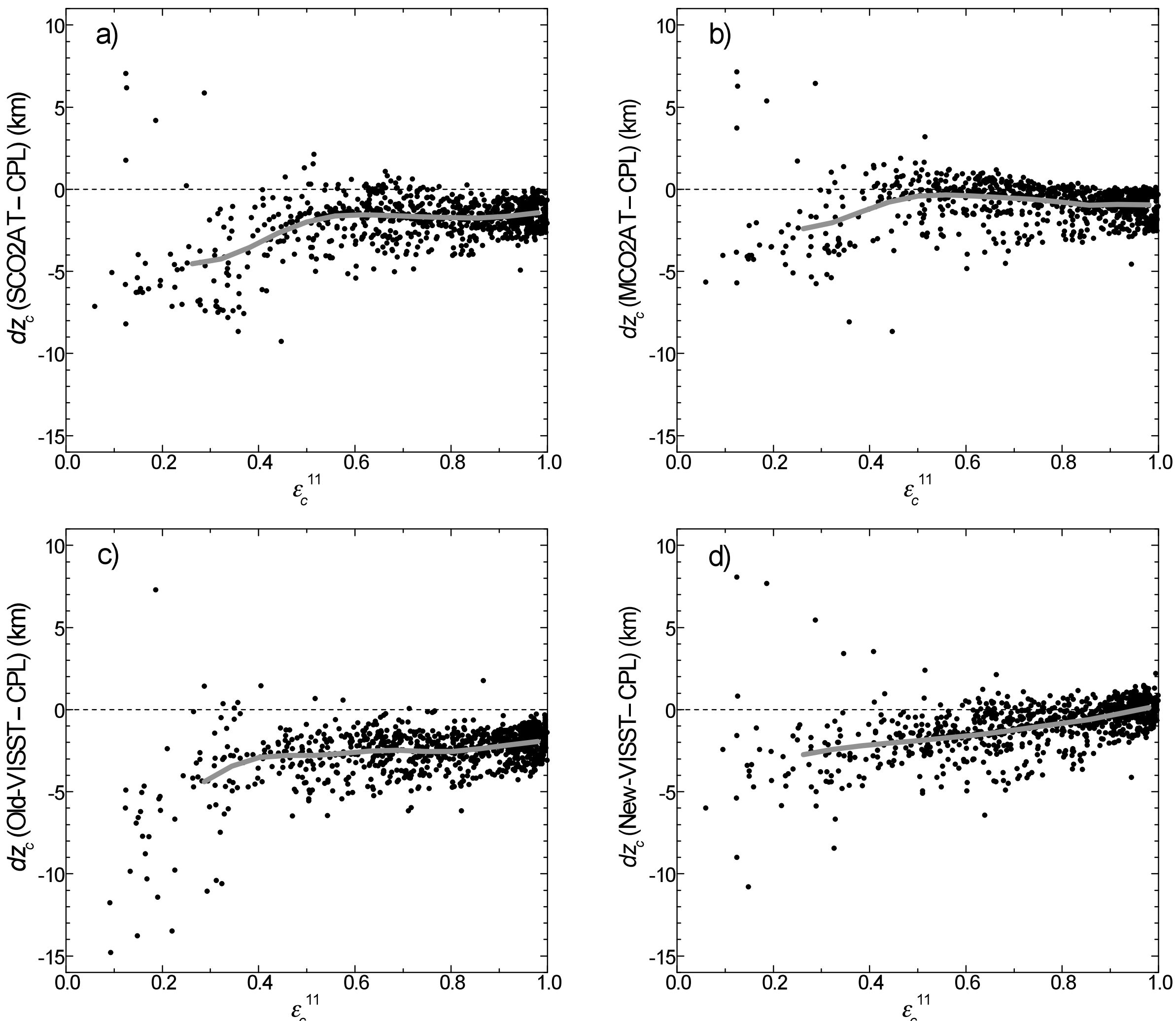

Fig. 6 Same as in Fig. 4, except for the single-layered clouds.

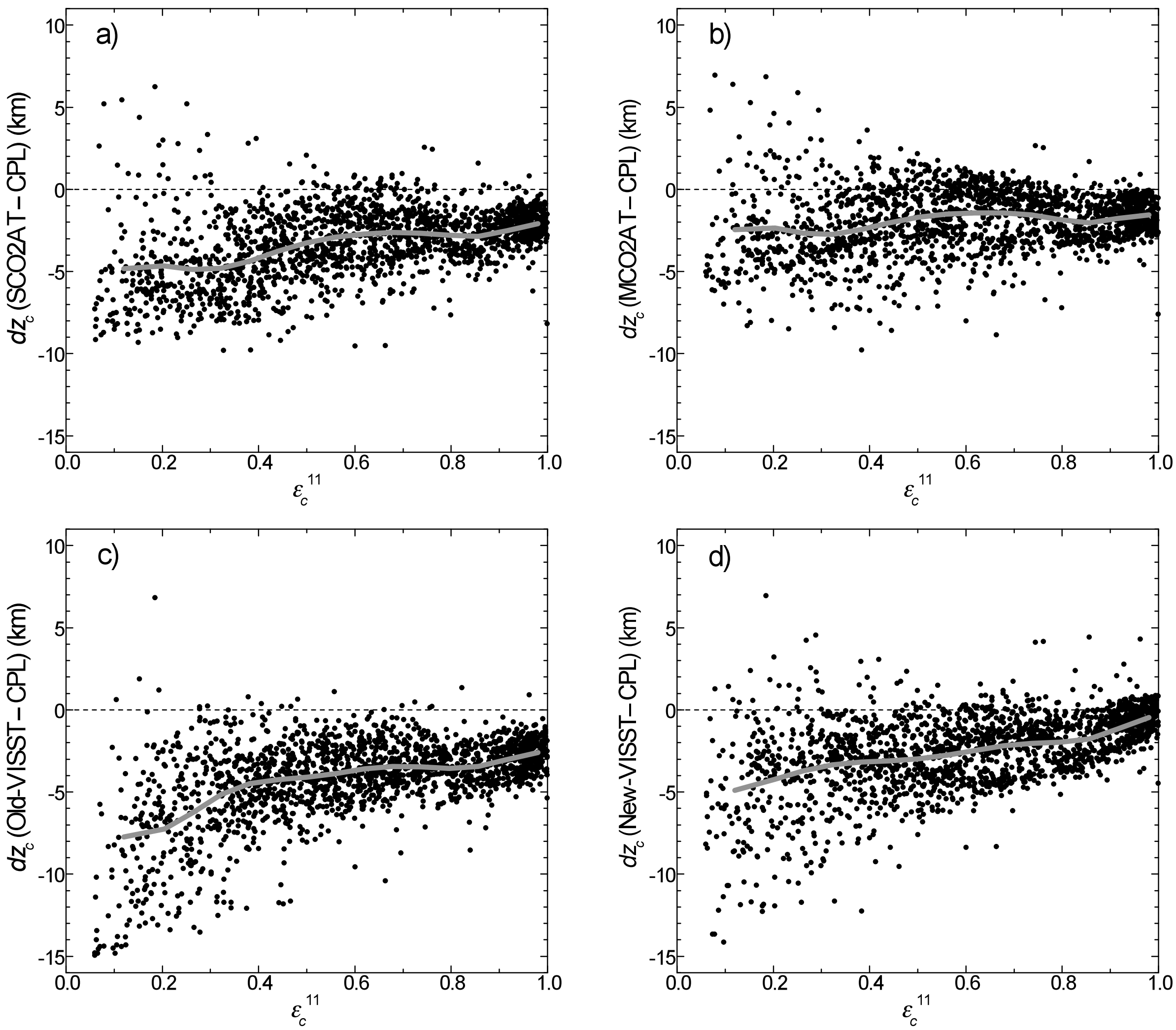

Fig. 7 Same as in Fig. 4, except for the two-layered clouds.

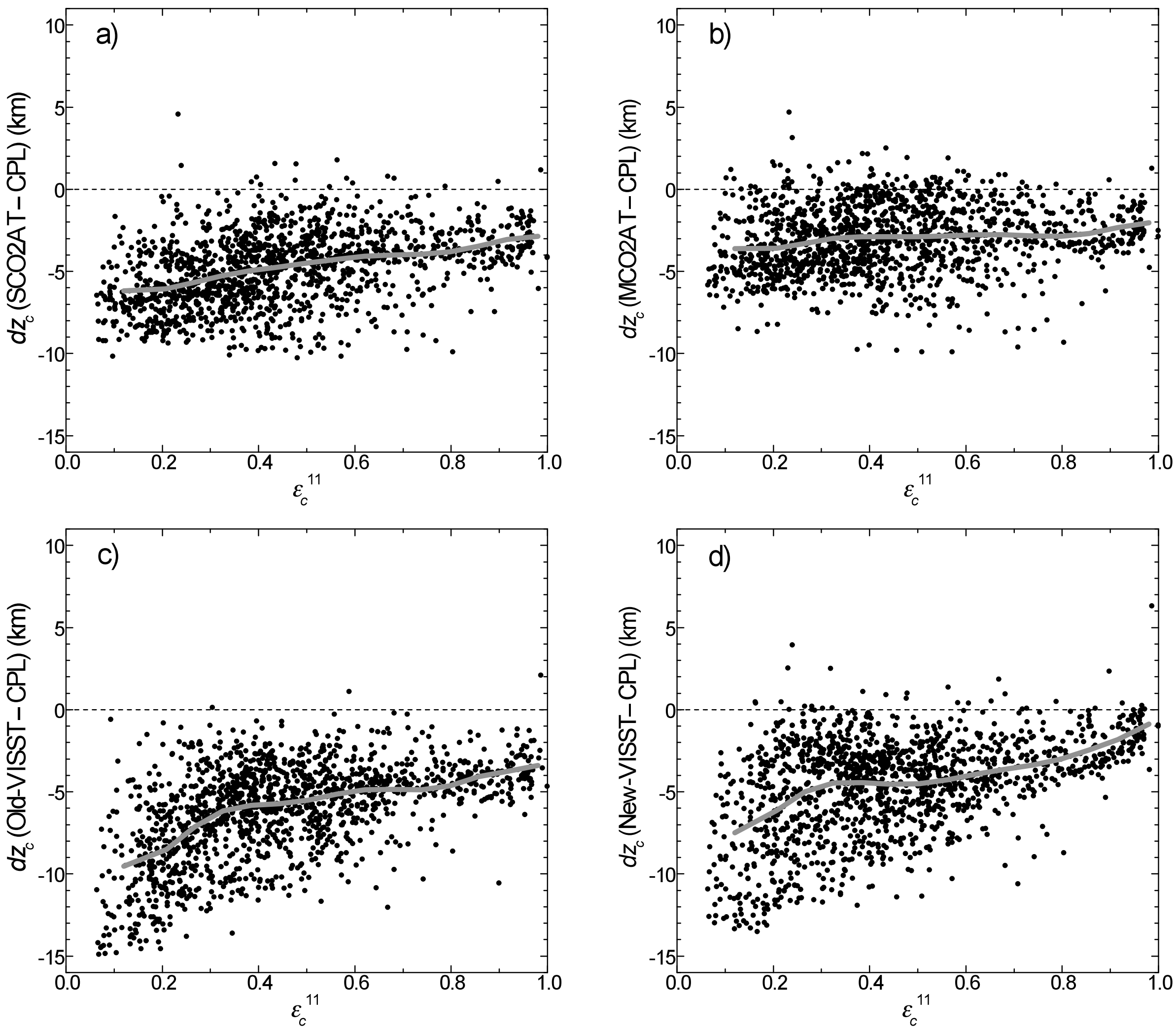

Fig. 8 Same as in Fig. 4, except for the multilayered ($N_{layer} > 2$) clouds.

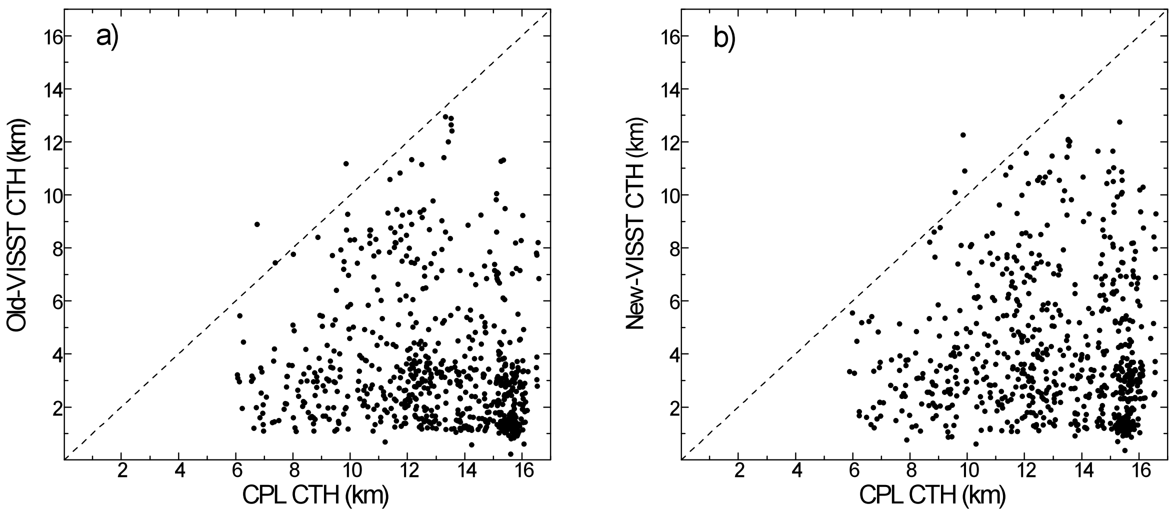

Fig. 9 Comparisons of the old-VISST (a) and new-VISST (b) CTHs with the CPL CTH for the data when there are no SCO2AT/MCO2AT retrievals.